19th Australasian Tunnelling Conference – Acosta-Martínez, Stewart and Hudson-Smith (Eds.)

Insights into the load transfer mechanisms of grouted rock bolts under tension

A. Emadi
SMEC, Australia

A. RA Gomes
Tunnels and Underground Engineering, SMEC, Australia

ABSTRACT: This study investigates load transfer mechanisms among bolt, grout and rock in fully-grouted rock bolts subjected to axial tension, both before and after bolt yielding. For that, a three-dimensional ABAQUS finite-element model is used to explicitly simulate bolt ribs, incorporating an elasto-plastic material model for steel, Concrete Damage Plasticity for grout, and interface interactions defined by hard contact in the normal direction and tangential behavior using the penalty method with friction. After validating the model against published pull-out tests, parametric analyses are conducted to assess the impact of rib height and spacing in the system behavior. Results show that load is progressively transferred from steel to grout, with peak stresses becoming nearly uniform along the anchorage at maximum load. Failure occurs through a coupled mechanism: grout cracking initiates at rib corners and propagates diagonally to form a conical shear band, accompanied by localized bolt yielding. Increasing rib height improves peak capacity and post-yield ductility up to ≈1 mm, beyond which benefits taper off. Conversely, excessively tight or wide rib spacing reduces energy absorption or strength. It has also been demonstrated that standard bond-slip models calibrated for reinforcing bars underestimate peak load and soften prematurely, as they neglect interlock and confinement effects.
These findings offer a micromechanical basis to refine simplified design models and optimize rib geometry for balanced strength and ductility in underground reinforcement systems.

1 LITERATURE REVIEW

Efficient load transfer in fully-grouted rock bolts hinges on the coupled response of steel, grout, and rock, with shear strength at the bolt–grout and grout–rock interfaces controlling system stability. Three-dimensional FE studies in Abaqus (e.g., Ho et al., 2019) model this behavior, typically combining an elasto-plastic steel law with Concrete Damage Plasticity for grout to capture cracking, plastic flow, and stiffness loss validated against pull-out tests.

Once slip initiates, strain incompatibility at the steel–concrete interface reduces axial stiffness and increases bolt displacement. To represent this bond–slip behavior, several studies have introduced equivalent interface models—most notably those proposed in FIB Bulle-tin 70 (2014)—that employ simplified traction–separation laws or cohesive elements. Parametric analyses (Cao et al., 2014; others) show that rib spacing, height, shape, and in-situ confinement dictate peak bond strength, post-peak softening, and the sequence of load-transfer stages.

Together, the literature underscores a complex interplay among material properties, rib design, and geology; capturing these interactions, especially beyond bolt yielding, is vital for reliable underground reinforcement.

2 VERIFICATION PROCEDURE

As a first step, the numerical model is verified against experimental results to ensure that its mechanical behavior and modelling assumptions accurately reflect test conditions. For this study, the pull-out tests conducted by Benmokrane et al. (1995) are simulated in Abaqus. The model reproduces the actual geometry - including bolt ribs - and boundary conditions. As shown in Figure 1a, the concrete cylinder has a diameter of 200mm and a height of 340 mm; a 38 mm-diameter borehole is drilled at its center. A deformed bolt with a core diameter of d = 15.8 mm and a rib height of h_a = 1.1 mm is grouted into the borehole using hardened cement paste at various embedment lengths. A steel plate placed at the top of the specimen prevents axial displacement of both grout and concrete during testing.

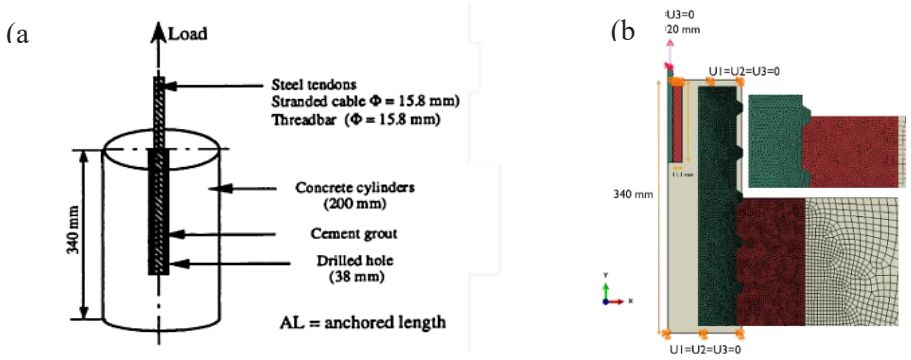

Figure 1. a) Schematic of the concrete cylinder test setup (Benmokrane et al. (1995)); b) Axisymmetric numerical model of pull-out tests conducted by Benmokrane et al., with a zoomed- in view of the discretized elements and boundary condition.

The key material properties of the steel bolt are: Young's modulus = 210 GPa and a Poisson's ratio=0.3. The grout is modelled using the Concrete Damage Plasticity (CDP) model, where, after initial debonding, the bolt-grout interface is represented by a frictional coefficient of μ=0.4. Figure 1b shows the axisymmetric finite-element model and the discretization details.

Figure 2 compares the load-displacement response obtained from the numerical model with the experimental model curve. The close agreement between the two confirms the accuracy and reliability of the modelling methodology.

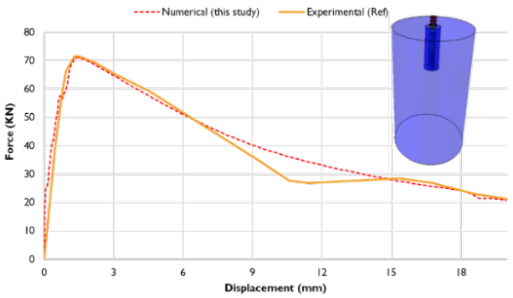

Figure 2. Comparison of the numerical model and experimental load-displacement curves.

3 PARAMETRIC STUDY

After model validation, parametric analyses were conducted varying rib height (0.5, 1.0, 2.0 mm) and spacing (7.25, 14.5, 29 mm). The simulations tracked stress evolution at different pull-out test stages to assess the impact of rib arrangement and the validity of equivalent models, such as the bond-slip model proposed by FIB and empirical formulas.

3.1 *Geometry and material properties*

Based on the actual shape of the threaded steel rock bolt, the transverse rib plays a crucial role in the load transfer mechanism and can influence the bolt's failure mode. To establish a realistic reference model for subsequent parametric studies, the numerical model includes a bolt rod with a 20 mm diameter, featuring a 1.5 mm × 1 mm spline and spiral ribs with dimensions of 1 mm (height) × 1.5 mm (width) × 14.5 mm (spacing). The ribs are inclined at a 54-degree angle relative to the rod axis (Figure 3a). The borehole diameter is 44 mm, creating a grout annulus of 12 mm. The surrounding rock cylinder has a 100 mm diameter and a 500 mm length, while the bolt length is 300 mm. The overall geometry of the numerical model is shown in Figure 3b.

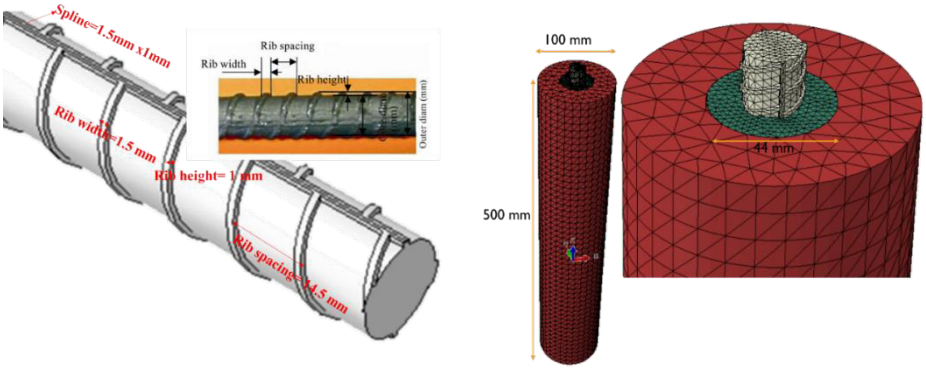

Figure 3. a) Geometric configuration of the rock bolt, D=20 mm. b) Geometry of the numerical model with a zoomed-in view of the discretized elements.

The steel bolt is modelled as an elasto-plastic material with strain hardening. Its key material properties include a Young's modulus of 210 GPa, a Poisson's ratio of 0.3, and a yield stress of 450 Mpa. The grout parameters considered in the CDP model are presented in Table 1, where E is the Young's modulus, v is the Poisson's ratio, fc Is the uniaxial compressive strength, f_t is the tensile strength, ψ is the angle of dilatancy and e is the eccentricity. The ratio fb/fc0, represents the biaxial-to-uniaxial compressive strength, defined as per ABAQUS CDP recommendations. The grout and steel bolt parameters considered in this study are representative of typical values found in common engineering practice, ensuring the relevance of the findings to real-world application.

Table 1.Grout parameters used in the CDP model

Parameter	E (GPa)	Density(Kn/m3)	ν	fc (MPa)	f_t (MPa)	e	K	ψ (°)	fb/fc_0
Value	25.8	23	0.15	51.8	4.2	0.1	1.12	30	1.12

In Abaqus, the parametric model incorporates surface interaction defined by normal behavior using hard contact, and tangential behavior modeled with the penalty method and a friction coefficient of 0.4. The rock is modeled using the Mohr-Coulomb failure criterion. Its mechanical properties consist of a Young's modulus of 6000 MPa, a Poisson's ratio of 0.25, a density of 24 kN/m³, a friction angle of 50°and cohesion of 500 kPa. In the model, a fixed boundary condition is applied to the outer surface of the rock cylinder, fully constraining all degrees of freedom.

3.2 *Analysis of Pull-Out Test Results and Stress Distribution*

Figure 4 presents the results of the pull-out test. The initial portion of the curve shows a steep, nearly linear increase in force from 0 to approximately 150 kN over a displacement of about 1 mm, indicating elastic deformation, where the rock bolt resists the applied load with minimal strain.

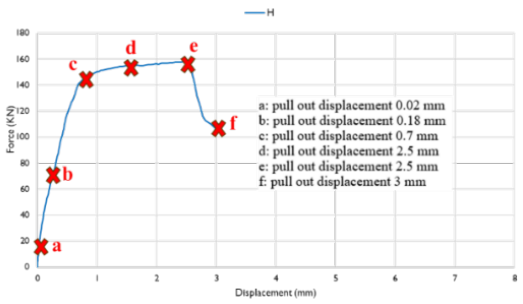

Figure 4. Load–displacement curve from reference pull-out test

Beyond this point, the curve begins to flatten, marking the onset of plastic deformation or yielding, with the force peaking at approximately 159 kN at a displacement of 2.5 mm. A sharp drop follows, with the force decreasing to around 100 kN at 3 mm displacement, likely indicating bond failure at the bolt-grout or grout-rock interface. After this stage, the curve stabilises around 100 kN, suggesting the presence of residual strength as the rock bolt continues to slide and deform.

Figure 5 illustrates the longitudinal normal and tangential stress distribution at the steel/grout interface during different loading stages: before peak load (P_1 = 50 kN), at peak load (P_2 = 159 kN), and after peak load (t_3, P_3 = 120 kN). The stress profiles exhibit fluctuations that correspond to the bolt's rib spacing (14mm). As axial displacement increases, the influence of the ribs on the stress distribution becomes more pronounced, highlighting the role of bolt geometry in the bolt-grout interaction. Prior to peak load, the tangential stress (Figure 5b) gradually mobilizes from the bolt head along the interface. At peak load, although the tangential stress reaches its maximum and is mobilized over a greater length, localized fluctuations remain significant due to the mechanical interlocking between the ribs and the grout. Therefore, while the global trend of stress distribution becomes broader and more mobilized, the stress does not become completely uniform along the interface.

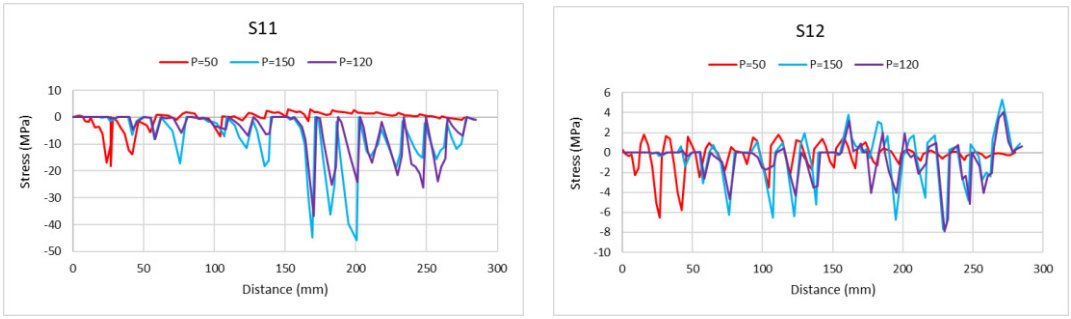

Figure 5. Longitudinal distribution of stresses (a) Normal stress s11 (b) Tangential stress s12.

Figures 6 and 7 illustrate the progressive failure mechanisms during a simulated pull-out test, as captured by the evolution of Plastic Strain Equivalent (PEEQ) and Tensile Damage (DAMAGE-T) across six distinct stages (a–f), revealing a coupled failure mechanism involving both grout cracking and bolt yielding. It should be noted PEEQ is a non-negative scalar that indicates the accumulated plastic strain and is used to identify regions of plastic deformation.

In the initial stages of displacement (Figures 7a–b and 8a–b), the rock bolt remains elastic while tensile cracks nucleate at rib corners near the loaded end and grow longitudinally as load transfers from steel to grout.

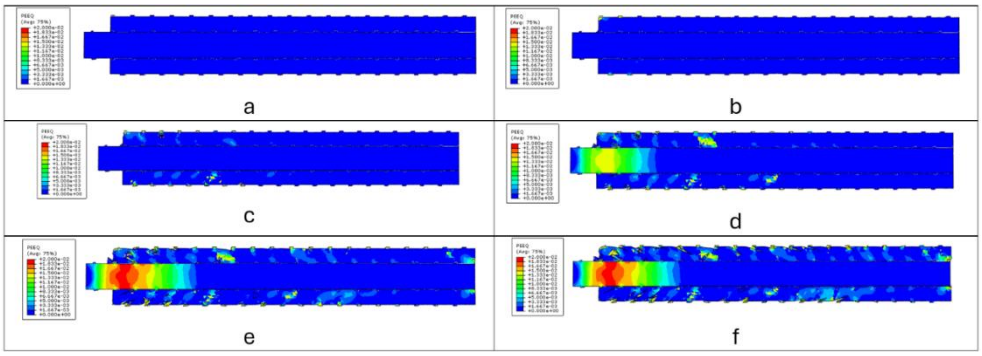

Figure 6. evolution of plastic strain equivalent (PEEQ) in the rock bolt model.

During the subsequent stages (Figures 7c–e and 8c–e), tensile damage extends progressively along the anchorage length. A distinct fracture path initiates at an angle of approximately 60° to the bolt axis (stage b), which gradually evolves into a conical shear failure inclined at roughly 45°. This transition reflects the influence of compressive stress concentrations at the rib angles, guiding crack propagation in alignment with orientations of maximum tensile stress. At the same time, plastic strain in the bolt increases, indicating the onset of local steel yielding.

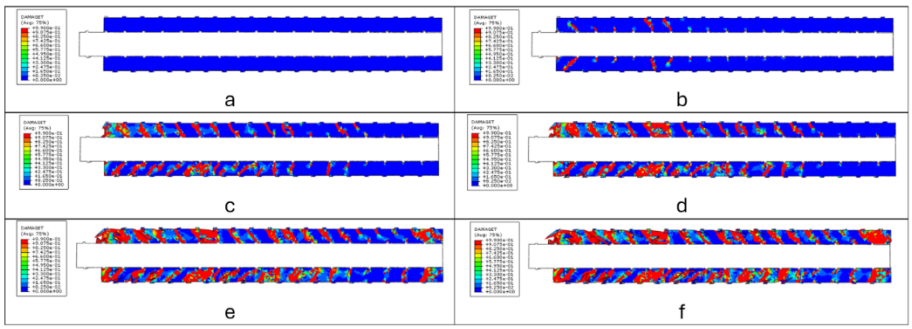

Figure 7. Evolution of the tensile damage (DAMAGE-T) of grout in the rock bolt model.

In the final stage (Figures 7f and 8f), extensive damage is observed in the grout, which coalesces into a shear band. This leads to the complete loss of load transfer and eventual pull-out of the rock bolt. The initiation of cracks at the rib corners and subsequent diagonal propagation confirm that transverse ribs play a critical role in dictating the failure paths. It is important to note that the failure observed in this model arises from the combined effects of grout degradation and bolt yielding, rather than either mechanism acting independently.

3.3 *Rib height and space*

A numerical simulation study was conducted with rib height and rib spacing as key variables. The modeling process considered three rib heights (0.5 mm, 1 mm, and 2 mm) and three rib spacings (7.25 mm, 14.5 mm, and 29 mm). Table 2 presents the analyses cases along with the corresponding rib height and rib spacing.

Table 2. Analyses cases with corresponding rib heights and rib spacings

Analyses case	Rib height (mm)	Rib Spacing (mm)
H or S	1	14.5
0.5H	0.5	14.5
2H	2	14.5
0.5S	1	7.25
2S	1	29

Figure 8 illustrates the equivalent plastic damage observed under different transverse rib heights and spacings. When the transverse rib height is 0.5 mm, cracks extend fully along the rock bolt, leading to complete bond failure and bolt disengagement. At greater rib heights, the failure mechanism changes significantly: the rock bolt remains more securely anchored and does not pull out. Instead, yielding occurs at the front end, with cracks appearing at the interface near the transverse ribs. As rib height increases, the mechanical coupling effect at the interface is enhanced, shifting the failure mode from abrasion, expansion, and rib sliding to rib body shearing and interface crack propagation. When rib spacing is too large, the number of transverse ribs along the bolt decreases, limiting their reinforcing effect and preventing full stress mobilization. Conversely, excessively small rib spacing can lead to cracks in the grout forming too closely together, which reduces the anchoring efficiency of the ribs.

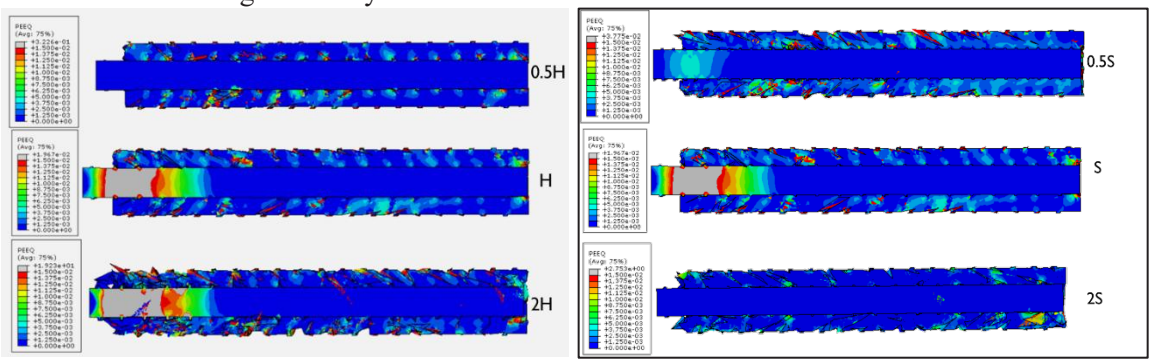

Figure 8. equivalent plastic strain under different transverse rib heights and spacings all subfigures use the same contour range with a maximum displayed value of 0.015; values exceeding this are shown in gray.

Figure 9 presents the load–displacement curves for rock bolts with varying transverse rib heights and spacings. The results show that for rib heights of 0.5 mm, 1mm, and 2.0 mm, the ultimate anchorage-bearing capacities are 136kN, 159kN, and 162kN, respectively. Increasing rib height from 0.5 mm to 1 mm, yields a 15% improvement in bearing capacity. However, as rib height increases further, the rate of improvement gradually diminishes.

It is also observed that as rib height increases, failure occurs at a later stage under tensile loading, indicating enhanced post-yield performance and improved load transfer capacity. This occurs because smaller ribs offer less mechanical interlocking and reduced frictional resistance at the interface, weakening the interface's ability to resist shear failure. These findings confirm that mechanical engagement and frictional resistance are critical to the load-bearing capacity of the transverse ribs. As displacement increases, smaller ribs are less effective at maintaining interlock, resulting in weaker anchorage performance of the rock bolt.

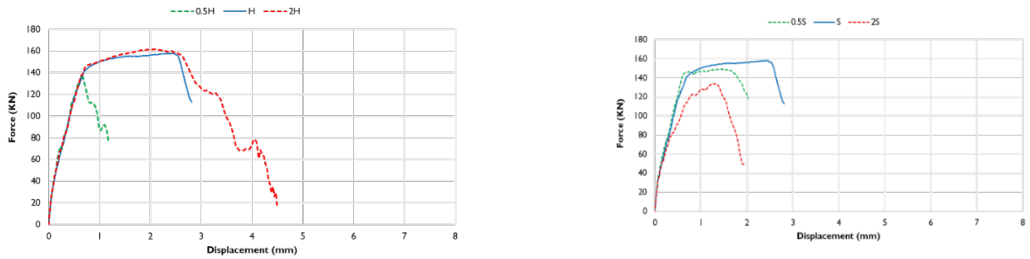

Figure 9. Load–displacement curve for different rock bolt transverse rib heights (left) and spacings (right).

The results indicate that for rib spacings of 7.25 mm, 14.5 mm, and 29 mm, the ultimate bearing capacities are 149 kN, 159 kN, and 132 kN, respectively. The load–displacement curves show that as transverse rib spacing increases, the peak load gradually decreases. While the three curves exhibit similar peak capacities, the improvement with reduced spacing become marginal beyond a certain density (e.g., below 15 mm). This suggests that increasing rib density beyond a threshold does not significantly increase the peak bond strength.

The 7.5 mm spacing (green), although achieving a peak load similar to reference model, shows a steeper post-peak drop, indicating lower energy absorption and a more brittle failure mode. When ribs are too closely spaced (e.g., 7.5 mm), the grout between ribs becomes too thin, and interlocking zones begin to interfere with each other. This results in premature shear failure of the thin grout layers, limiting the system's ability to develop distributed slip and plastic deformation.

The outcome is localized shear damage, loss of confinement, and reduced overall ductility of the rock bolt system.

3.4 *Empirical methods (equivalent interface models)*

Three different modeling approaches were considered to simulate the interaction between bolt and grout:

a) the base model with explicit rib geometry (blue solid line),
b) the FIB-based bond-slip model (red dashed line), and;
c) the equivalent bond-slip model with modified parameters and mesh (gray solid line).

To simulate the interaction between bolt and grout, bond-link elements are employed. These elements have no physical dimensions and connect two coincident nodes via nonlinear springs (Figure 10). By assigning appropriate force–displacement relationships to these springs, the bond–slip behavior at the concrete–rebar interface can be accurately captured. Initially the parameters used for bond-slip relationship are defined using the equation provided in Table 6.1.1 of the FIB Model Code, corresponding to confined concrete under favorable bond conditions.

Figure 10. Schematic representation of bond-link elements modeling the rebar–grout interface using four dimensionless nonlinear springs per interval

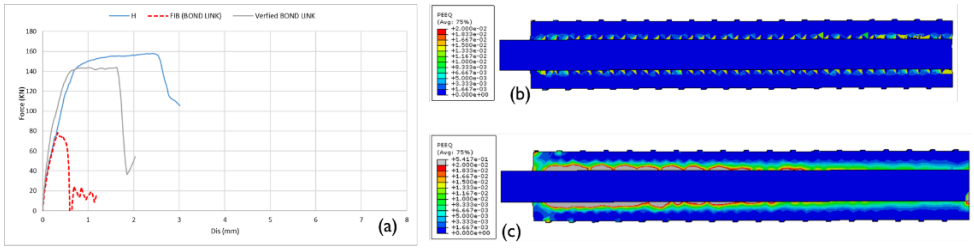

Figure 11. a) Comparison of load-displacement curves for base model (explicit rib geometry), FIB-based bond-slip model, and modified bond-slip model b) PEEQ distribution in FIB-based bond-slip model showing minimal grout plasticity with no steel plasticity c) PEEQ distribution in modified bond-slip model showing distributed grout plasticity but no steel plasticity

Figure 11 presents the load-displacement curves for each one of the modelling approaches. The FIB-based model shows a peak load of approximately 80 kN, substantially lower than the 160 kN achieved with the explicit base model. The peak load capacity of the modified bond-slip model is in the same order of magnitude of the based model, though with slightly different post-peak behavior. The plastic equivalent strain (PEEQ) distributions reveal fundamental differences in failure mechanisms between the modeling approaches. The base model shows concentrated plastic deformation in both the grout around the bolt ribs and in the steel bolt itself, indicating a combined failure mechanism involving both materials. In contrast, both bond-slip models (Figure 11) show plastic deformation exclusively in the grout, with no plasticity observed in the steel bolt component. The FIB-based bond-slip model exhibits minimal plastic deformation, with damage primarily concentrated at the grout-bolt interface in discrete bands. The modified bond-slip model shows more distributed plastic deformation throughout the grout volume but still fails to capture the steel

plasticity observed in the reference model. These results demonstrate that while bond-slip models can be calibrated to match the overall load-carrying capacity, they fail to accurately capture the complex failure mechanisms associated with ribbed rock bolts in grout. Although the bond–slip model is based on standard formulations, such as those in the FIB Model Code for reinforcing bars in concrete, it fails to capture the mechanical interlock and confinement effects induced by the rib geometry of rock bolts embedded in grout. It is important to emphasize that the FIB Model Code is primarily calibrated for reinforcing rebars in concrete structures and may not accurately capture the behaviour of rock bolts in grout.

4 SCOPE AND LIMITATION

The findings presented in this study are based on the specific geometric and material parameters of the reference model. Variations in bolt and rib geometry, grout properties, confinement conditions, or loading rates may result in different load transfer behaviors and failure patterns.

5 CONCLUSIONS

Based on the analyses conducted, the following key findings can be highlighted:

- Stress distribution: FE analysis shows that rib geometry significantly influences stress along the bolt–grout interface, producing periodic fluctuations. Although the overall mobilization of tangential stress increases at peak load, the stress distribution remains locally non-uniform.
- Failure mechanism: Cracking initiates at rib corners, then propagates diagonally through the grout, forming shear bands controlled by rib geometry and local confinement condition; failure is a coupled mechanism involving both grout cracking and bolt yielding.
- Rib height: Increasing rib height enhances bond strength and post-yield performance; however, improvements diminish beyond 1 mm. Taller ribs tend to shift the failure mechanism from rib abrasion or sliding to rib body shearing and interface cracking. In contrast, ribs with 0.5h height showed lower bond capacity due to reduced mechanical interlock and frictional resistance compared to the baseline and larger rib cases.
- Rib spacing: Very tight spacing (≈ 7.25 mm) produces brittle, localized shear due to thin grout layers and overlapping interlock zones, while wide spacing (≈ 29 mm) lowers capacity by reducing the number of effective ribs. Below ~15 mm, extra ribs offer little additional peak strength.
- Load–displacement response: Rib geometry governs both peak capacity and ductility; optimal spacing and height balance strength with energy absorption.
- Bond–slip models: Bond-slip models, while computationally efficient, demonstrate significant limitations in capturing the complex failure mechanisms of ribbed rock bolts in grout.
- Design implication: Detailed micromechanical modelling might be recommended to inform design decisions of high-performance rock bolt systems, especially in complex conditions.
- Scope: Findings apply to the reference model; other parameter variations may yield different load transfer behaviors and failure patterns.

6 REFERENCES

Benmokrane, B., Chennouf, A. and Mitri, H.S., 1995, October. Laboratory evaluation of cement-based grouts and grouted rock anchors. In International journal of rock mechanics and mining sciences & geomechanics abstracts (Vol. 32, No. 7, pp. 633-642). Pergamon.

Cao, C., Ren, T., Cook, C. and Cao, Y., 2014. Analytical approach in optimising selection of rebar bolts in preventing rock bolting failure. *International Journal of Rock Mechanics and Mining Sciences*, *72*, pp.16-25.

Ho, D.A., Bost, M. and Rajot, J.P., 2019. Numerical study of the bolt-grout interface for fully grouted rockbolt under different confining conditions. *International Journal of Rock Mechanics and Mining Sciences*, *119*, pp.168-179.